Chapter 4

Fabrication and Characterization of Pd/ZnO Nanoparticles based Schottky Diode for NO_2 Sensing at Room Temperature

4.1 Introduction

Research on the gas sensing arena has been widely explored over the past few years globally, for detection of toxic, hazardous, greenhouse, ozone depleting and air polluting gases. Nitrogen dioxide (NO_2) is one of the most toxic, ozone-depleting gas (Portmann, Daniel and Ravishankara, 2012) and need immediate detection as it is very harmful to human health and the environment. NO_2 causes formation of photochemical smog and acid rain (Urasinska-Wojcik *et al.*, 2017), degradation in body immune system, nervous system (Navale *et al.*, 2014) and the respiratory system. NO_2 gas is generally emitted due to the combustion of fuels in automobiles, excessive use of pesticides and insecticides in agriculture (Thu *et al.*, 2017), aquatic sapling, home heaters, industry, and furnaces etc. It has thus compelled the researchers to detect even low concentration ($\leq$ 10 – 100 ppb) (Valentini *et al.*, 2003; Xia *et al.*, 2008) of NO_2 gas. Several types of NO_2 gas sensors (like resistor, capacitor, diode, transistor etc.) (Filippini *et al.*, 2001; Andringa *et al.*, 2012; Miyoshi, Fujita and Egawa, 2015; Urasinska-Wojcik *et al.*, 2017) have been developed and commercialised but most of these sensors are very complex in structure, difficult to recover, and need higher operating temperature in general.

Material plays very crucial and important role for detection of various gases for improving the response and increasing the fidelity toward selective gases. Nowadays, semiconductor metal oxides (WO_3, SnO_2, ZnO etc.) are promising candidates for detection of various gases (Sadek *et al.*, 2007; Rai and Yu, 2012; Rai *et al.*, 2012; Shim *et al.*, 2014; Van Quang *et al.*, 2014) with good sensitivity. However, ZnO possesses the significant advantages

among all the other materials such as – high electron mobility, good thermal and chemical stability (Xu *et al.*, 2008), low cost, large exciton binding energy (60 meV) (Özgür *et al.*, 2005), and easy to prepare numerous morphological nano-structures (Comini, 2006; Kumar *et al.*, 2014). The nanostructure of the ZnO thin film has led to numerous adsorption site, large pore size and high surface to volume ratio etc. which increase the interaction of gas molecules to the sensor's surface, results increase in sensitivity.

The higher temperature operation of such sensors possesses the requirement of necessary heating the device and has become a bottleneck for the development of IC compatible sensor. The studied Schottky diode mostly uses Pd owing to its excellent capability of adsorption towards NOx molecules (Huang, Long and Yang, 2001). Penza *et al.* (Penza, Martucci and Cassano, 1998) have been reported that the highest NOx response based on Pd film in comparison to Au and Pt noble metal. Besides this, Pd consists of good selectivity toward NOx with respect to various gases (CO, CH_4, SO_2, H_2S, and NH_3 etc.) (Penza, Martucci and Cassano, 1998). Therefore, in the present work, an effort has been made to develop Pd/ZnO on a glass substrate for detection of NO_2. The developed sensor has shown very good sensitivity for NO_2 detection at room temperature. The observed results have been explained in terms of surface and subsurface adsorption of NO_2 on Pd and subsequent diffusion through catalyst Pd to Pd/ZnO interface. This gives rise to the formation dipole formation at Pd/ZnO interface. In addtion, the side diffusion of NO_2 is also expected for observed high detection sensitivity.

4.2 Diode Fabrication and Characterization Tools

In order to fabricate and characterize the Pd/ZnO nanoparticles based Schottky diode upon exposure to NO_2 the instruments and facilities availed in the laboratory has been discussed below:

4.2.1 Vacuum Thermal Evaporation Unit

The vacuum thermal evaporation unit having model no.: 12A4D (Hindhivac Co. Ltd., India, make) is shown in Figure 4.1. In the vacuum deposition process, the material (to be deposited) is thermally vaporized by applying a high potential difference across the tungsten filament where the material is kept in the presence of high vacuum. The vacuum chamber is made of electrochemically-polished stainless steel and consists of a circular glass window which enables visuals of the ongoing deposition process. Vacuum is created by a diffusion pump and double stage driven rotary vacuum pump. The pressure is measured by the Pirani and Penning gauge. The Pirani gauge measures the pressure in the range from 0.5 to 10^{-3} Torr and Penning gauge measures in the range 10^{-3} to 10^{-6} Torr. The Pirani gauge is used to measure roughing and backing pressure and the penning gauge is used to measure lower pressure in the chamber.

Figure 4.1: Front view of Hindhivac 12A4D thermal evaporator.

4.2.2 Thermo Chuck

The Thermo chuck (model TP 36, Temptronics Corporation make) has shown in Figure 4.2 which consists of a 3-probe system along with a temperature controller. Temperature is controlled with the help of a thermistor which is coupled to the thermo-chuck surface. The analog temperature indicator is attached with a thermo-chuck by which the low and high temperature can be observed. It has a timer also on the front panel, which can hold the temperature for a particular time and a can also set the elapsed time. This model has an accuracy of ± 6 °C and the stability of ± 1 % in the chuck temperature (°C).

Figure 4.2: Front view of Thermo-chuck-system.

4.2.3 Spin Coater

Spin coater (Model no. SPM 150 LC, TSE systems) is shown in Figure 4.3. It is a thin-film deposition tool by which film is deposited on the flat substrate using spin coating technique. This coater is allowed of spinning from 500 to 8000 rpm. Usually, a small amount of coating material is applied at the center of the substrate. The centrifugal force disperses the coating material over the whole substrate. The thin layer is deposited by repeating steps of spin coating process.

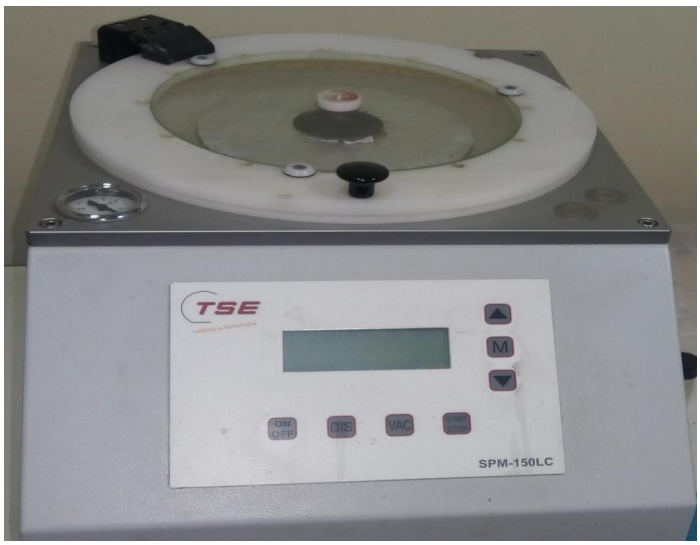

Figure 4.3: Front view of a spin coater.

4.2.4 Bench furnace

The bench furnaces (model no.: MB71, Thermco Inc., USA) is illustrated in Figure 4.4. It has three independent furnaces:

(i) Furnace for oxidation

(ii) Furnace for annealing

(iii) Furnace for diffusion

The furnace consists of Ana-lock (model 431) general purpose temperature controller with a temperature range of 200 to 1200 °C with $\pm$ 15 °C accuracy. The muffled cylindrical tubes length of 14 inches and outer diameter of 3.25-inch are fitted inside the uniformly heated flat zone furnace. The nickel-chromium-aluminum wire as the heating element is wounded helically over the tube gauge. Water cooling is also provided to the heating chamber so that heat can be removed approximately 60 % of the BTU (British thermal unit) in order to operate the furnace otherwise the heat would dissipate into the laboratory. Besides water cooling, air cooling is also coupled through silent running, high volume circulating fans, which draw the room air to keep all the running components trouble free even at the maximum operating temperature rating.

Figure 4.4: Front view of Bench furnace.

4.2.5 Measurement Equipment

This section covers the brief explanation of instruments those has been used during the measurements of device electrical and physical characteristics.

4.2.5.1 Ellipsometer

Ellipsometer, of model L117 (Gaertner Scientific Corp., Chicago, USA) is widely used for measuring the thickness and refractive index of the film. A front view of the ellipsometer is shown in Figure 4.5. It consists of a light source having He-Ne 6328 *Å* LASER of 2 mW power which projected 1 mm diameter spot on the surface. It has a polarizer and analyzer at the left and right respective side. The polarizer is used in order to generate linearly polarized light from He-Ne laser which passes through the compensator. As the light reflects from the sample, the polarization of the light becomes change accordance to the film thickness and optical characteristics of the film and substrate. The light then passes

through the analyzer and is sensed by the photodetector. The amount of the laser light reaching the photodetector is indicated by extinction-meter. The extinction meter or detector has a built-in solid-state amplifier. At a certain polarizer angle, the analyzer is rotated to a position where almost no light reaches the photodetector. This will enable to measure the obtained data with the data sheet provided by the company.

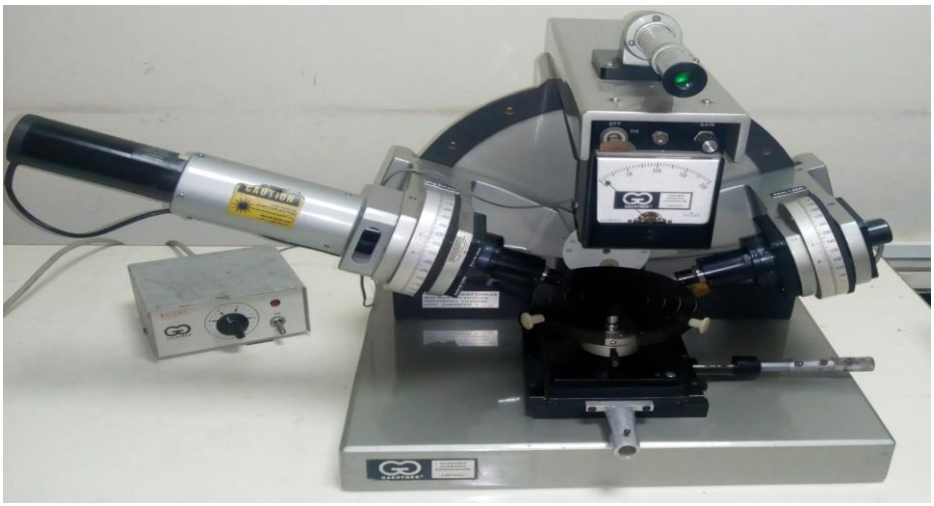

Figure 4.5: Front view of L117 Gaertner Scientific Corporation ellipsometer.

4.2.5.2 Semiconductor Parameter Analyzer

The semiconductor parameter analyzer (Model no. B1500A) as shown in Figure 4.6 is an electronic instrument that performs multiple measurements such as the current-voltage (I-V) and capacitance-voltage (C-V), capacitance-frequency (C-f) and pulse/dynamic IV etc. The key measurement component of the B1500A is a Sources Measure Unit (SMU). The SMU is a measurement module that combines the capabilities of a voltage/current source and a voltage/current meter into a single module. This analyzer typically measures the I-V including low current measurement up to fA (femto amperes) resolution and C-V measurements up to 1 MHz. The compliance of current in this analyzer is 50 mA sharply.

Figure 4.6: Front view of semiconductor parameter analyzer.

4.3 Experiment Details

The fabrication of Pd/ZnO Schottky diode is accomplished on the glass substrate using thin film technology. The fabrication steps for Pd/ZnO nanoparticles based Schottky diode is shown in Figure 4.7.

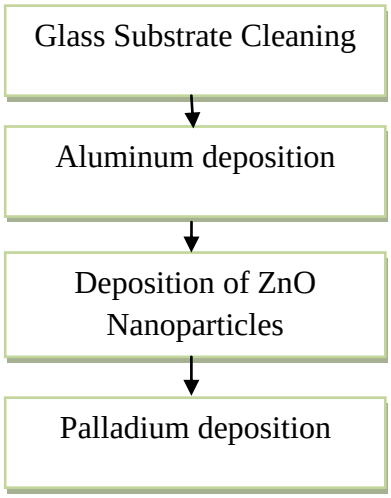

Figure 4.7: Flowchart of the fabrication of Pd/ZnO nanoparticles based Schottky diode.

The glass substrate of having a dimension (15 mm x 15 mm) was ultrasonically cleaned using soap solution, acetone, and propanol respectively. After-that, the aluminum metal was deposited (~ 70 nm) over a cleaned glass substrate by a thermal evaporation

technique. In the next step, the synthesized ZnO nanopowder (~ 0.2 g) (synthesis process has been discussed in chapter 3) was dispersed into 10 ml methanol solvent and then this was stirred vigorously for 2 h. The spin coater was used to deposit ZnO film on already prepared Al electrode over a glass substrate. The ZnO nanopowder solution was repeatedly spin coated at a rotation speed of 3000 rpm for 25 sec and subsequently was kept in an electric oven at 150 ºC for 10 min. This process was repeated 10 times. The grown film was annealed in N_2 ambient at 400 °C for 2 h. The thickness of deposited ZnO film was around 250 nm confirmed by the ellipsometer (GAERTNER Scientific Corporation, serial no. 806-AI). To complete the device structure Pd was deposited (~ 40 nm) over ZnO thin film using the thermal evaporation technique and subsequently annealed at 450 °C for 7 min. A cross-sectional view of the fabricated Pd/ZnO device is shown in Figure 4.8.

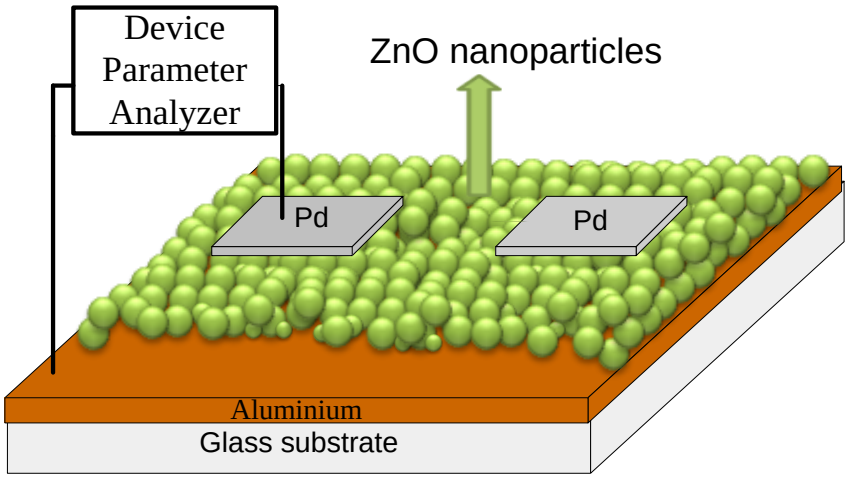

Figure 4.8: Schematic of Pd/ZnO nanoparticles based Schottky diode.

4.4 Sensing Characterization of Pd/ZnO Schottky Diode

The detection sensitivity for NO_2 of the developed sensor has been studied using the experimental set-up as shown in Figure 4.9. The set-up consists of an airtight stainless steel test chamber of 10,000 cc volumes with the provision of gas inlet-outlet. To measure the

response, SUT (sensor under test) was kept in the chamber and connected to a parameter analyzer (keysight B1500A). Keysight B1500A measures the I-V characteristics of SUT upon exposure of NO_2 (purity 99.99 %, purchased by Sigma-Aldrich). NO_2 was injected into the test chamber through a scaled syringe. I-V characteristic was recorded with as increase in NO_2 concentration (10 – 50 ppm). Afterward, the sensor was exposed to air through outlet valve for recovery. The NO_2 concentration was calculated by the Equation (4.1)

$$NO_2 \text{ Concentration (ppm)} = \frac{NO_2 \text{ Concentration (Liter)}}{\text{Closed Chamber Volume (Liter)}} \quad (4.1)$$

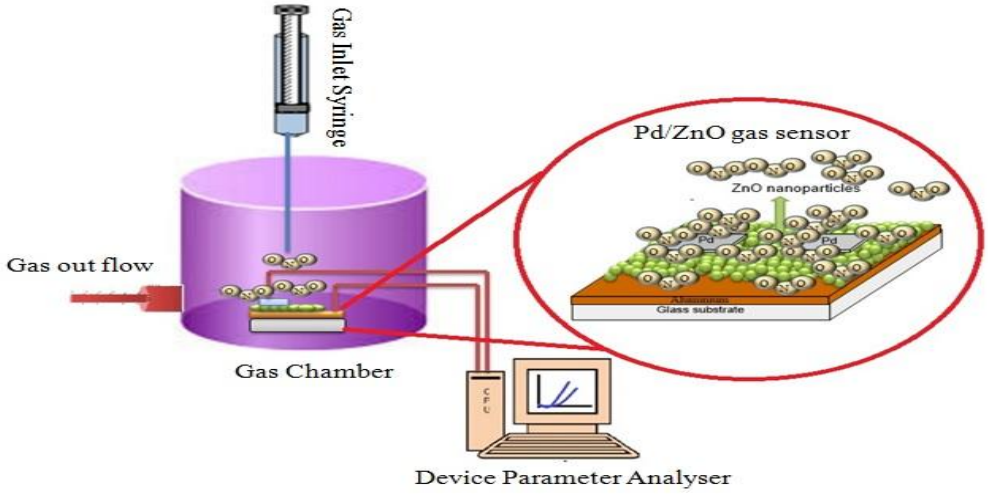

Figure 4.9: Schematic diagram of NO_2 measurement set-up.

4.5. Results and Discussions

The result and discussion section describe the structural, electrical and gas sensing properties of the fabricated Pd/ZnO sensor.

4.5.1 Structural Results

The phase formation, purity, and crystallinity of ZnO film were investigated using X-ray diffraction pattern (XRD) (Shim *et al.*, 2014). Figure 4.10 (a) shows the XRD pattern of ZnO film. The crystallite size of ZnO NPs was found to be ~ 19.91 nm using Scherrer's formula $D = 0.89\lambda/(\beta\cos\theta)$, where λ is the radiation wavelength of 0.154 nm which was generated by Cu-Kα X-ray source, β represent the full width at half-maximum (FWHM) and θ is called as diffraction angle (Eriksson *et al.*, 2009; Srivastava, Gusain and Sharma, 2013; Elangovan *et al.*, 2015). The peak intensity was found along (100), (002), (101), (102), (110), (103), (200), (112) and (201) at 2θ angles 31.79º, 34.42º, 36.26º, 47.55º, 56.62º, 62.9º, 66.4º, 68º, 69.14º respectively. The specific 2θ angle and their intensities of the diffraction peaks are confirmed by the powder diffraction standards data (JCPDS No. 36-1451) (Yi *et al.*, 2007). The XRD pattern reveals that ZnO NPs are polycrystalline with a hexagonal structure. The surface morphology of grown film was analyzed by Atomic Force Microscopy (AFM) in 5 µm scale range as shown in Figure 4.10 (b). This AFM image reveals that the average roughness ~ 52.73 nm and its roughness mean square (RMS) is 66.50 nm

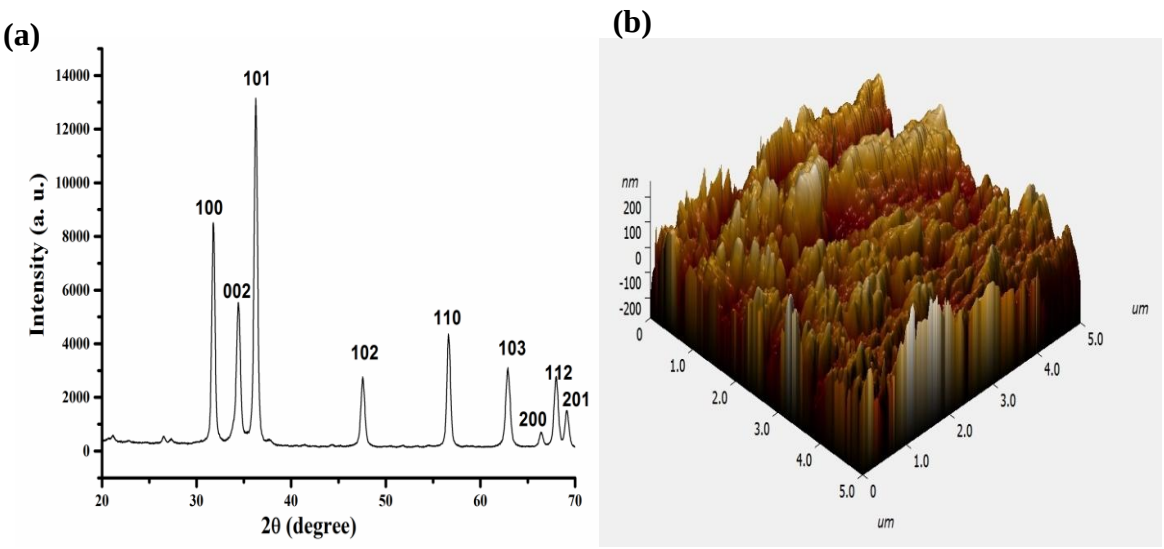

(c) **(d)**

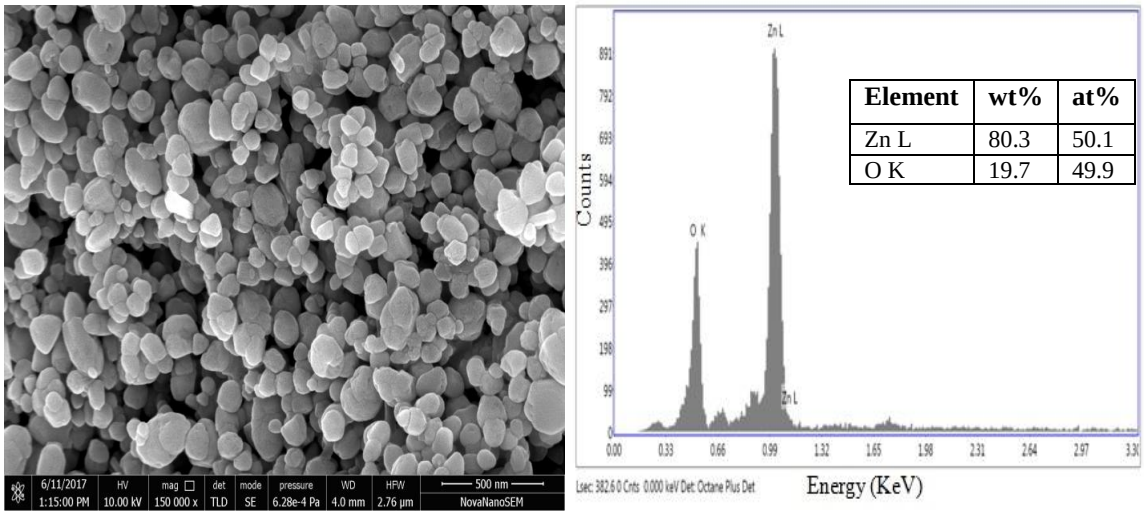

Element	wt%	at%
Zn L	80.3	50.1
O K	19.7	49.9

Figure 4.10: (a) XRD (b) AFM (c) FE-SEM and (d) EDS image of 2 h annealed film of ZnO NPs at 400 ºC.

The particles size of ZnO NPs based film were investigated by field emission scanning electron microscopy (FE-SEM) (Eriksson *et al.*, 2009). Figure 10 (b) depicts the surface morphology of 2 h. annealed ZnO NPs based film at 400 °C in 500 nm scaling range. It reveals the numerous ZnO NPs ranging from ~ 25 nm to ~ 110 nm. This particles range concludes the average particles size ~ 42 nm. Figure 4.10 (d) shows the energy dispersive X-ray spectroscopy (EDS) of the ZnO NPs based film. This spectrum was measured from 0 to 3 keV (in X-axis) which confirms the presence of zinc (Zn) and oxygen (O) elements in the synthesized nanoparticles. Absorption peaks depict the highest strength of zinc (Zn) element followed by oxygen (O) element with wt % 80.3, 19.7 and at % 50.1, 40.9 respectively.

4.5.2 NO_2 Sensing Results

I-V characteristic of Pd/ZnO NPs based Schottky diode was characterized using semiconductor device parameter analyzer (Keysight B1500A). Figure 4.11 (a) shows the forward and reverse biased (-1 to 1 V) I-V characteristics of Pd/ZnO Schottky structure which confirms the Schottky junction at Pd/ZnO interface. The rate of charge flow in

Schottky diode can be described by thermionic emission theory which gives the forward current (I) by Equation (4.2) (Aydoğan *et al.*, 2009; Rajan *et al.*, 2017)

$$I = I_0 \left[\exp\left(\frac{qV}{\eta kT}\right) - 1\right] \quad (4.2)$$

Where η is ideality factor, k is Boltzmann constant 1.38 x 10^{-23} J/K, T is operating temperature in Kelvin, V is applied forward bias voltage, q is an electronic charge, and I_0 is the reverse saturation current of Pd/ZnO Schottky diode. I_0 is calculated using $\ln(I)$ vs V plot in low bias (0 to 0.5 V) by linear interception at zero volt (Chiu *et al.*, 2009). The other dependent parameter is ideality factor (η) which can be easily calculated by the Equation (4.3) (Rajan *et al.*, 2017)as shown below.

$$\eta = \left\{\frac{q}{kT}\right\} \times \left\{\frac{\partial V}{\partial \ln(I)}\right\} \quad (4.3)$$

Where, η is extracted from the slope of the linear region of $\ln(I)$ vs V plot shown in Figure 4.11 (a) in low bias (0 – 0.5 V) (Rajan *et al.*, 2017). The most important parameter of Schottky diode is barrier height (Φ_B) or Schottky junction height which can be calculated through the relation given Equation (4.4) (Yadav, Pandey and Jit, 2014; Rajan *et al.*, 2017)

$$q\emptyset_B = kT \ln\left(\frac{AA^{**}T^2}{I_0}\right) \quad (4.4)$$

Where A is the effective contact area of diode 15 mm^2, A** is effective Richardson constant 32 A-cm^{-2} K^{-2} at room temperature (298 K) (Al-Ghamdi, Al-Heniti and Mahmoud, 2013; Kaphle and Hari, 2016) which is the standard value for ZnO. These all electrical parameters of Pd/ZnO Schottky diode have easily been modulated according to the NO_2 concentration at room temperature. The Table 4.1 shows the change in barrier height (Φ_B), ideality factor (η)

and reverse saturation current (I_0) with a change in NO_2 concentration ranging from 10 to 50 ppm. Figure 4.11 (b) shows the increase in barrier height (Φ_B) from ~ 0.675 eV to ~ 0.727 eV and ideality factor from ~ 3.175 to ~ 5.608.

Table 4.1: Change in diode parameters with a variation of NO_2 concentration.

NO_2 Conc. (in ppm)	**Barrier height (φ_B in eV)**	**Ideality factor (η)**	**Reverse current (I_0 in nA)**
0	0.675	3.175	16.17
10	0.687	3.521	10.31
20	0.694	3.714	7.95
30	0.707	4.117	4.67
40	0.721	5.282	2.78
50	0.727	5.608	2.17

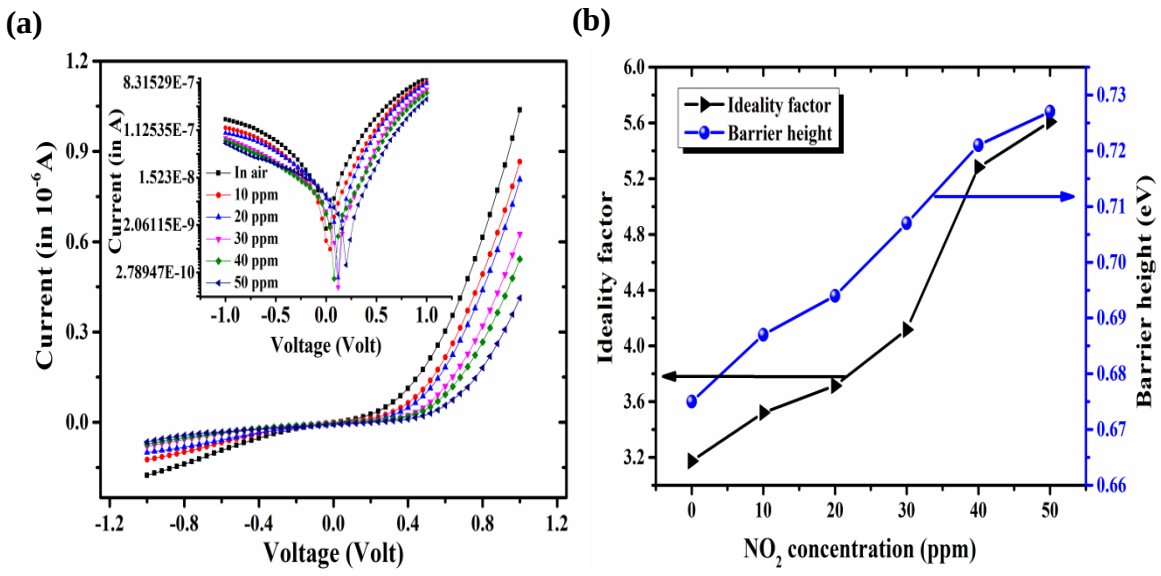

Figure 4.11: (a) I-V characteristics of Pd/ZnO diode. The inset shows the ln(I) vs V plot. (b) Change in ideality factor and barrier height upon exposure to NO_2 concentration ranging from 10 to 50 ppm at room temperature.

The change in current of Pd/ZnO sensor upon exposure of NO_2 gas can be explained as follows: when Pd/ZnO sensor exposed to the air, the environmental oxygen adsorbs to the Pd

surface and then diffuse to the ZnO surface (Basu *et al.*, 2008; Das *et al.*, 2010). These oxygen atoms are chemisorbed to ZnO surface and forming oxygen ions which act as a created trap sites for NO_2. The nanostructure of the ZnO enhances the trap site of the surface due to large surface to volume ratio. On the other hand, when NO_2 exposed to Pd/ZnO Schottky contact, the flow of charge carrier can be briefly described by following three steps as shown in Figure 4.12. In the first step, upon exposure of NO_2 to Pd/ZnO sensor, the NO_2 molecules become adsorbed on the surface and subsurface of Pd metal (Bishop *et al.*, 2015) and dissociates into nitric oxide and oxygen (NO+O) atom (Talazac *et al.*, 2004; Hemminger, 2006; Chiang *et al.*, 2010; Bishop *et al.*, 2015) as shown in Figure 4.12 (a). In the second step, Figure 4.12 (b) shows the dissociated atoms further diffuse to Pd/ZnO interface. Finally in the third step, the diffused atoms is chemisorbed (Talazac *et al.*, 2004; Bishop *et al.*, 2015) through available superficial trapped charges (oxygen ions) (Bishop *et al.*, 2015; Usha, Mishra and Gupta, 2015) on ZnO NPs at Pd/ZnO interface and give rise in dipole moments as shown in Figure 4.12 (c). These dipole moments leads to barrier height ($\Phi_{B,NO2}$) and corresponding work function ($\psi_{m,NO2}$) of Pd which reduces the transportation of charge carrier through Pd/ZnO junction. The change in barrier height ($\Delta\ \Phi_B = \Phi_{B,NO2} - \Phi_{B,air}$) occurs according to Equation (4.5) (Chiu *et al.*, 2009; Bishop *et al.*, 2015)

$$\Delta\ \Phi_B = \frac{\mu N_i \theta_i}{\varepsilon_s} \qquad (4.5)$$

Where μ is effective dipole moments, N_i is the number of sites per area at the interface, θ_i is the coverage of an oxygen atom at the interface. These augmentations of barrier height results in increase in ideality factor of Pd/ZnO Schottky diode. Further, when the exposed gas release, diffused atoms tries to eject from the Pd catalyst. This ejection of atoms reduces the dipole moment at Pd/ZnO interface which results in decreases in barrier height. Practically,

the diffused atoms are not ejected completely from Pd, results not exact recovery of barrier height occurs.

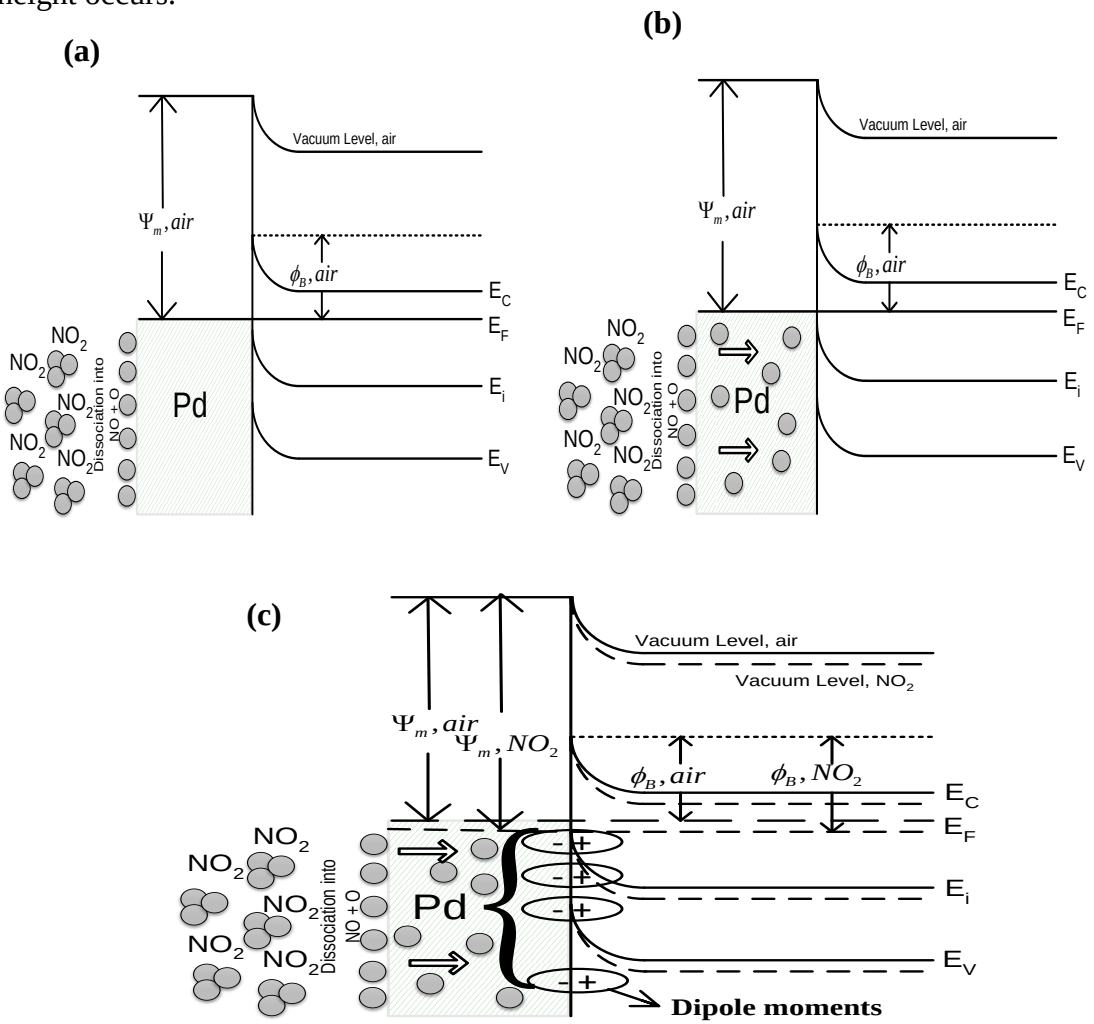

Figure 4.12: Energy band diagram representation of Pd/ZnO Schottky diode upon exposure to NO_2 shows (a) adsorption (b) diffusion (c) formation of dipole moments results change in diode parameters.

The sensitivity (S) of the developed sensor has been defined by Equation (4.5) (Bishop *et al.*, 2015; Thu *et al.*, 2017)

$$S\ (\%) = \frac{I_{air} - I_{NO_2}}{I_{air}} \times 100 \qquad (4.5)$$

Where, I_{air}, is diode forward current in air and I_{NO_2} is the diode forward current on the various NO_2 gas concentration (10 – 50 ppm) operating at room temperature. It was observed that the NO_2 response increases with increase in NO_2 concentration (10 – 50 ppm) as shown in transient response in Figure 4.13 (a).

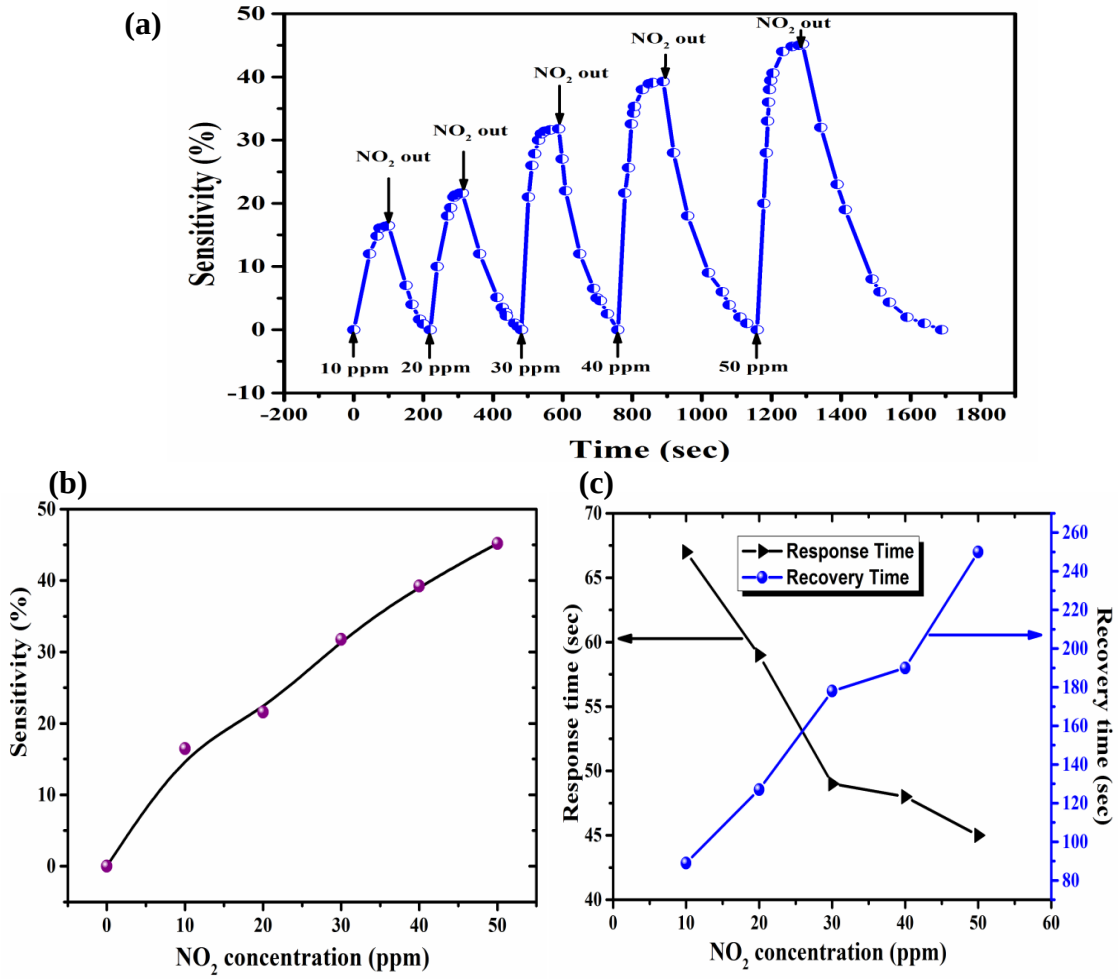

Figure 4.13: (a) Transient response of Pd/ZnO Schottky sensor (b) Sensitivity plot (c) response and recovery time of Pd/ZnO sensor upon NO_2 concentration ranging from 10 to 50 ppm at room temperature.

Figure 4.13 (b) shows the increase in percentage sensitivity ~ 16.71%, ~ 21.6% and ~ 31.78%, 39.25% and ~ 45.2% upon exposure of NO_2 10, 20, 30, 40 and 50 ppm respectively. The lower sensitivity occurs at a low concentration of NO_2 molecules (~ 10 ppm) due to less

formation of dipole moment layer at the interface. On another hand, higher sensitivity occurs due to higher diffusion of NO_2 into Pd surface as well as side diffusion of NO_2 also results in a large number of dipole moments formations at larger available trap sites on Pd/ZnO interface. Figure 4.13(c) shows the plot of response and recovery time of the sensor upon exposure of NO_2 concentration from 10 to 50 ppm. The response time calculates as the time taken by the sensitivity to reach the value of 90 % of its peak value (Thu *et al.*, 2017) and similarly recovery time measured by the time is taken by sensitivity to fall back to 90 % (Kadhim, Abu Hassan and Abdullah, 2016; Thu *et al.*, 2017) or 10 % of maximum value. It is observed that, as NO_2 concentration increases, the response time decreases (67 to 45 s). This drastic change appears due to the availability of large surface and subsurface adsorption sites on the Pd surface. However, the recovery time is found to increase from 89 to 250 seconds respectively; most probably due to trapped dipole moment not leaving the surface immediately. Figure 4.14 shows the three consecutive time sensor's sensitivity under the same NO_2 concentration of 10 ppm and reveals the response of ~ 16.47%, ~ 15.18% and ~ 15.92% operating at room temperature. It concludes that the fabricated sensor produces an excellent repeatable response.

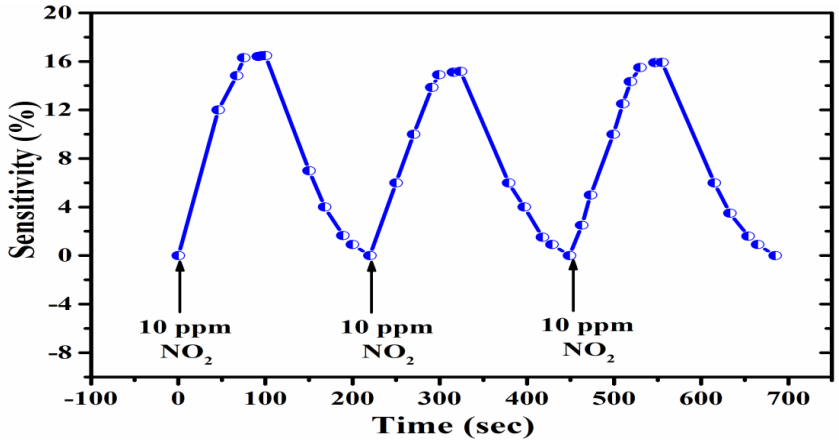

Figure 4.14: The repeatable transient response of Pd/ZnO sensor under 10 ppm NO_2 gas.

4.6 Conclusion

The chapter 4 discusses the available facilities in the laboratory such as vacuum thermal evaporator, spin coater, bench furnace and ellipsometer etc. which has been used for diode fabrication and characterization. Furthermore, this chapter has discussed the development of Pd/ZnO nano-particles based Schottky diode on a glass substrate for NO_2 detection. The ZnO film was characterized by FESEM, EDS, XRD and AFM which reveals the wurtzite structure of ZnO having nanoparticles size range from ~ 25 to ~110 nm with surface roughness around 52.73 nm. I-V characteristic of diode upon exposure of NO_2 concentration ranging from 10 to 50 ppm was investigated in the voltage range from - 1 to 1 V. The sensitivity of the sensor has been studied with varying concentration of NO_2 from 10 to 50 ppm and obtained values are ~ 16 to ~ 45.2 % with excellent repeatability. The possible cause of obtaining sensitivity is believed to be the creation of an interfacial dipole layer at Pd/ZnO interface due to variation in the NO_2 concentration. These interface dipole moments provide an additional increase in the barrier height from ~ 0.675 eV to ~ 0.727 eV and ideality factor from ~ 3.175 to ~ 5.608 both. These appealing features of fabricated Pd/ZnO diode make an attractive sensor capable of NO_2 detection at low concentration with fast response and recovery time, which is an important consideration for any gas sensing device. This fabricated sensor is not only cost-effective but also presents a highly stable response.

References

Al-Ghamdi, S. A., Al-Heniti, S. H. and Mahmoud, W. E. "Schottky barrier effect of ZnO modified methyl glycol thin films for detection of hydrogen sulfide gas", *Ceramics International*, 2013, vol. 39, pp. 5025–5030.

Andringa, A. M. *et al.* "Dynamics of charge carrier trapping in NO2 sensors based on ZnO field-effect transistors", *Sensors and Actuators, B: Chemical*, 2012, vol. 171–172, pp. 1172–1179.

Aydoğan, Ş. *et al.* "Electrical characterization of Au/n-ZnO Schottky contacts on n-Si", *Journal of Alloys and Compounds*, 2009, vol. 476, no. 1–2, pp. 913–918.

Basu, P. K. *et al.* "Low temperature methane sensing by electrochemically grown and surface modified ZnO thin films", *Sensors and Actuators, B: Chemical*, 2008, vol. 135, pp. 81–88.

Bishop, C. *et al.* "Highly sensitive detection of NO2 gas using BGaN / GaN superlattice-based double Schottky junction sensors", *Applied Physics Letters*, 2015, vol. 106, p. 243504.

Chiang, Y. T. *et al.* "The impact of TiO2interface layer on a Pd/n-LTPS schottky diode hydrogen detecting performances", *IEEE Transactions on Electron Devices*, 2010, vol. 57, no. 8, pp. 2013–2018.

Chiu, S. Y. *et al.* "Comprehensive investigation on planar type of Pd-GaN hydrogen sensors", *International Journal of Hydrogen Energy*, 2009, vol. 34, pp. 5604–5615.

Comini, E. "Metal oxide nano-crystals for gas sensing", *Analytica Chimica Acta*, 2006, vol. 568, no. 1–2, pp. 28–40.

Das, S. N. *et al.* "Fabrication and Characterization of ZnO Single Nanowire-Based Hydrogen Sensor", *J. Phys. Chem*, 2010, vol. 114, pp. 1689–1693.

Elangovan, S. V. *et al.* "Synthesis and characterization of sodium doped ZnO nanocrystals and its application to photocatalysis", *Superlattices and Microstructures*, 2015, vol. 85, pp. 901–907.

Eriksson, J. *et al.* "ZnO nanoparticles or ZnO films: A comparison of the gas sensing capabilities", *Sensors and Actuators B*, 2009, vol. 137, pp. 94–102.

Filippini, D. *et al.* "Field-effect NO2sensors with group 1B metal gates", *Sensors and Actuators, B: Chemical*, 2001, vol. 81, no. 1, pp. 83–87.

Hemminger, D. D. and J. C. "Decomposition of NO2 to NO and O on Pt (111)", *Surface Science*, 2006, vol. 241, no. 2, pp. 389–399.

Huang, H. Y., Long, R. Q. and Yang, R. T. "The Promoting Role of Noble Metals on NOx Storage Catalyst and Mechanistic Study of NOx Storage under Lean-Burn Conditions", *Energy & Fuels*, 2001, vol. 15, no. 1, pp. 205–213.

Kadhim, I. H., Abu Hassan, H. and Abdullah, Q. N. "Hydrogen gas sensor based on nanocrystalline SnO2 Thin Film grown on bare Si substrates", *Nano-Micro Letters*, 2016, vol. 8, no. 1, pp. 20–28.

Kaphle, A. and Hari, P. "Characterization of Aluminum Doped Nanostructured ZnO/p-Si Heterojunctions", *The International Journal Of Engineering And Science*, 2016, vol. 5, no. 10, pp. 2319–1813.

Kumar, R. *et al.* "Zinc oxide nanostructures for NO2 gas–sensor applications: A review", *Nano-Micro Letters*, 2014, vol. 7, no. 2, pp. 1–24.

Miyoshi, M., Fujita, S. and Egawa, T. "Demonstration of NOx gas sensing for Pd/ZnO/GaN heterojunction diodes", *Journal of Vacuum Science & Technology B, Nanotechnology and Microelectronics: Materials, Processing, Measurement, and Phenomena*, 2015, vol. 33, no. 1, p. 13001.

Navale, S. T. *et al.* "Room temperature NO 2 sensing properties of polythiophene films", *Synthetic Metals*. Elsevier B.V., 2014, vol. 195, no. 2, pp. 228–233.

Özgür, Ü. *et al.* "A comprehensive review of ZnO materials and devices", *Journal of Applied Physics*, 2005, vol. 98, no. 4, pp. 1–103.

Penza, M., Martucci, C. and Cassano, G. "NOx gas sensing characteristics of WO3 thin films activated by noble metals (Pd, Pt, Au) layers", *Sensors and Actuators B: Chemical*, 1998, vol.

50, no. 1, pp. 52–59.

Portmann, R. W., Daniel, J. S. and Ravishankara "Stratospheric ozone depletion due to nitrous oxide: influences of other gases", *Philosophical Transactions of the Royal Society B: Biological Sciences*, 2012, vol. 367, no. 1593, pp. 1256–1264.

Van Quang, V. *et al.* "Outstanding gas-sensing performance of graphene/SnO2 nanowire Schottky junctions", *Applied Physics Letters*, 2014, vol. 105, no. 1, p. 13107.

Rai, P. *et al.* "The role of gold catalyst on the sensing behavior of ZnO nanorods for CO and NO2 gases", *Sensors and Actuators, B: Chemical*, 2012, vol. 165, no. 1, pp. 133–142.

Rai, P. and Yu, Y. "Citrate-assisted hydrothermal synthesis of single crystalline ZnO nanoparticles for gas sensor application", *Sensors and Actuators B: Chemical*, 2012, vol. 173, no. 2, pp. 58–65.

Rajan, L. *et al.* "An Investigation on Electrical and Hydrogen Sensing Characteristics of RF Sputtered ZnO Thin-Film with Palladium Schottky Contacts", *IEEE Sensors Journal*, 2017, vol. 17, no. 1, pp. 14–21.

Sadek, A. Z. *et al.* "Characterization of ZnO nanobelt-based gas sensor for H2, NO2, and hydrocarbon sensing", *IEEE Sensors Journal*, 2007, vol. 7, no. 6, pp. 919–924.

Shim, Y. *et al.* "Chemical Highly sensitive and selective H2 and NO2 gas sensors based on surface-decorated WO3 nanoigloos", *Sensors & Actuators: B. Chemical*, 2014, vol. 198, no. 2, pp. 294–301.

Srivastava, V., Gusain, D. and Sharma, Y. C. "Synthesis, characterization and application of zinc oxide nanoparticles (n-ZnO)", *Ceramics International*, 2013, vol. 39, no. 8, pp. 9803–9808.

Talazac, L. *et al.* "Improvement in Sensitivity and Selectivity of InP-Based Gas Sensors: Pseudo-Schottky Diodes with Palladium Metallizations", *IEEE Sensors Journal*, 2004, vol. 4, no. 1, pp. 45–51.

Thu, D. T. *et al.* "Schottky contacts of (Au, Pt)/nanotube-titanates for fast response to NO2 gas at room temperature", *Sensors and Actuators B: Chemical*, 2017, vol. 244, pp. 941–948.

Urasinska-Wojcik, B. *et al.* "Ultrasensitive WO3gas sensors for NO2 detection in air and low oxygen environment", *Sensors and Actuators, B: Chemical*, 2017, vol. 239, pp. 1051–1059.

Usha, S. P., Mishra, S. K. and Gupta, B. D. "Fiber optic hydrogen sulfide gas sensors utilizing ZnO thin film/ZnO nanoparticles: A comparison of surface plasmon resonance and lossy mode resonance", *Sensors and Actuators, B: Chemical*, 2015, vol. 218, pp. 196–204.

Valentini, L. *et al.* "Sensors for sub-ppm NO2 gas detection based on carbon nanotube thin films", *Applied Physics Letters*, 2003, vol. 82, no. 6, pp. 961–963.

Xia, H. *et al.* "Chemical Au-doped WO3 based sensor for NO2 detection at low operating temperature", *Sensors and Actuators B*, 2008, vol. 134, no. 2, pp. 133–139.

Xu, J. *et al.* "Studies on alcohol sensing mechanism of ZnO based gas sensors", *Sensors and Actuators, B: Chemical*, 2008, vol. 132, no. 1, pp. 334–339.

Yadav, A. B., Pandey, A. and Jit, S. "Pd schottky contacts on sol-gel derived ZnO thin films with nearly ideal richardson constant", *IEEE Electron Device Letters*, 2014, vol. 35, no. 7, pp. 729–731.

Yi, S.-H. *et al.* "Low-temperature growth of ZnO nanorods by chemical bath deposition", *Journal of Colloid and Interface Science*, 2007, vol. 313, pp. 705–710.